

## Estimation of Ionospheric Electric Fields and Currents From a Regional Magnetometer Array

M. MURISON,<sup>1</sup> A. D. RICHMOND, AND S. MATSUSHITA<sup>2</sup>

*National Center for Atmospheric Research, Boulder, Colorado*

W. BAUMJOHANN<sup>3</sup>

*Max-Planck-Institut für Physik und Astrophysik, Institut für extraterrestrische Physik, Garching, Federal Republic of Germany*

We investigate the technique of calculating ionospheric electric fields and currents and field-aligned currents using an equivalent current function obtained from a regional array of ground-based magnetometers at high latitudes (Scandinavian Magnetometer Array). Like similar calculations previously done on a global scale, the derived electric fields and currents are found to depend on the model of ionospheric conductivity assumed. Unlike the global scale calculations, the regional calculations are also dependent on the assumed boundary conditions. Additional information on the electric fields, currents, and/or conductivities is required, besides the ground magnetic variations, to obtain unique estimations of the ionospheric electrodynamic features. In the present case, ionospheric drift measurements from one of the Scandinavian Twin Auroral Radar Experiment radars help constrain the calculations. Analysis of an equivalent current function at 1835 UT on October 7, 1976, representing Harang discontinuity conditions, suggests that upward field-aligned current probably existed near the boundary between eastward and westward electrojets.

### INTRODUCTION

The problem of determining the configuration of ionospheric and magnetospheric electric currents responsible for observed ground level magnetic perturbations has been a topic of continuing interest in geophysics. Although an infinite variety of three-dimensional current systems could produce any given magnetic perturbation field over the earth's surface, physical constraints will in practice greatly limit the current configurations that can be expected to exist. Current is known to flow primarily horizontally within the lower ionosphere at altitudes of 90–150 km and to flow primarily along the geomagnetic field direction above these heights, out to distances of several earth radii. Furthermore, the horizontal ionospheric current is believed to be approximately linearly related to an electrostatic field (Ohm's Law), with the conductivity tensor determined essentially to the accuracy of the variable ionic density of the lower ionosphere. Kern [1966] first showed that these physical constraints permit unambiguous determination of the three-dimensional current system from observed ground level magnetic observations over the earth if the ionospheric conductivity is horizontally uniform and if all current above the ionosphere is assumed to be radial. This latter assumption means that effects of distant magnetospheric currents like the ring current must first be removed from the data before applying Kern's [1966] procedure, but otherwise it is generally adequate, since most of the field-aligned current above the ionosphere flows at high latitudes where field lines are nearly radial. Several studies [e.g., Mishin and Popov, 1969; Fayermark, 1977; Levitin et al., 1977, 1982; Belov et al., 1978; Feldstein et al., 1982] have employed this procedure with simple,

horizontally uniform models of ionospheric conductivity together with observed magnetic perturbations over the northern hemisphere to estimate field-aligned current distributions under various geophysical conditions.

Matveev and Shpynev [1975] generalized Kern's [1966] method to allow for a nonuniform, but known, conductivity tensor. A primary difficulty in applying this generalized procedure is to devise a suitable conductivity model, especially for the auroral oval. Nevertheless, progress has been made in developing conductivity models and in using them to calculate ionospheric electric fields and currents and field-aligned currents for different conditions [e.g., Mishin et al., 1977, 1979, 1981; Bazarzhapov et al., 1979; Kamide et al., 1981; Kamide and Richmond, 1982, 1983; Feldstein et al., 1984; Friis-Christensen et al., 1985]. These calculations have had reasonable success for statistically averaged conditions, but the method has some difficulty when the actual conductivities are highly irregular and not well known, as is usually the case for individual instants of time [e.g., Kamide et al., 1982].

It is of interest to examine how well this type of procedure for analyzing geomagnetic measurements can be applied to data from a regional magnetometer array, as opposed to the global scale calculations discussed above. In this report we apply the method to data from the Scandinavian Magnetometer Array [Küppers et al., 1979] for a specific example representing the Harang discontinuity [Harang, 1946; Heppner, 1972]. The example we choose (October 7, 1976, 1835 UT) has been previously discussed by Baumjohann et al. [1978]. Simultaneous ionospheric electric field information is also available in the form of irregularity drift measurements by one of the Scandinavian Twin Auroral Radar Experiment (STARE) radars, as published by Baumjohann et al. [1978]. These irregularity drift measurements are fairly representative of the line-of-sight  $E \times B$  plasma drift velocity, at least for the moderate electric field magnitude of this example [Nielsen and Schlegel, 1983]. We make use of these measurements by comparing them with our calculated electric field to help verify the validity of our calculations and thus provide a constraint on our assumed input parameters.

<sup>1</sup>Now at Department of Astronomy, University of Wisconsin, Madison.

<sup>2</sup>Deceased.

<sup>3</sup>Formerly at Institut für Geophysik der Universität Münster, Federal Republic of Germany.

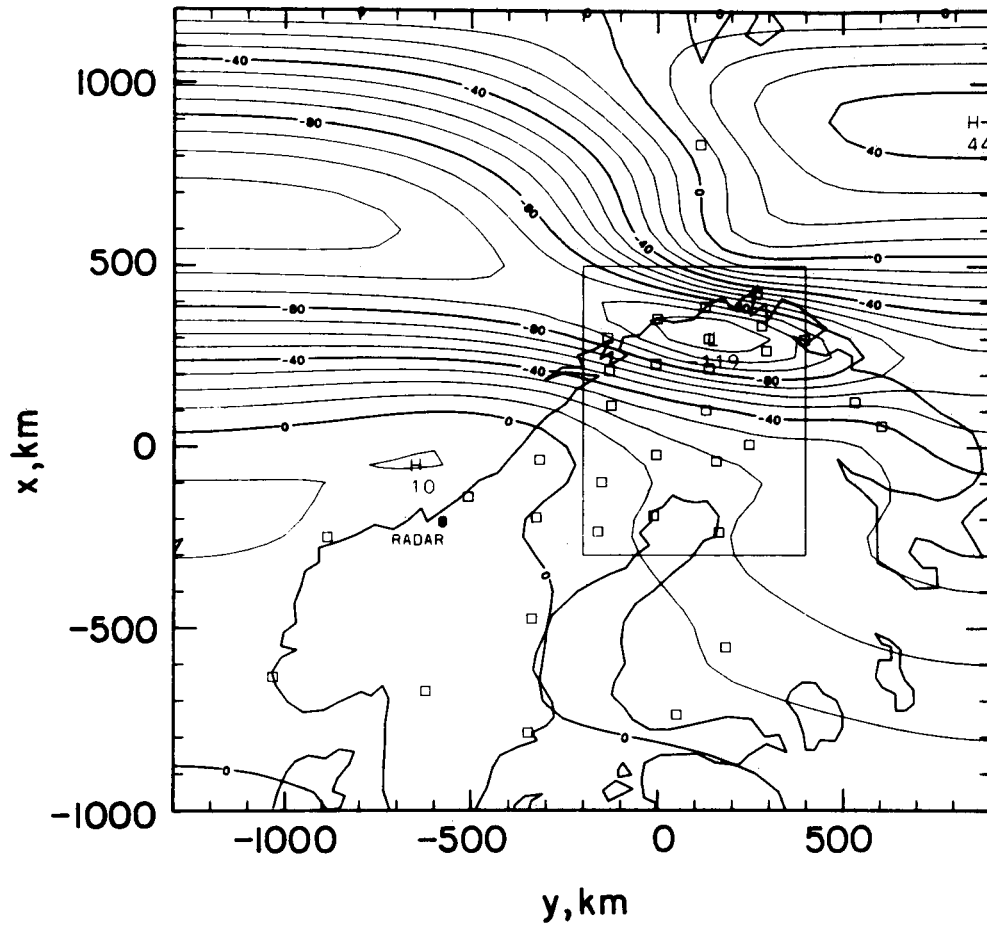


Fig. 1. Equivalent current function for October 7, 1976, at 1835 UT. The contour interval is 10 kA. Equivalent current flows counterclockwise around the minimum (L). Squares denote locations of magnetometers used to construct the pattern. The STARE radar used to measure ionospheric drifts is located at the circled star. The horizontal Kiruna coordinates are  $x$  and  $y$  (see text). The inner rectangle shows the region for which electrodynamic parameters are plotted in Figure 2.

#### COMPUTATIONAL PROCEDURE

The first step of the analysis is to estimate an ionospheric equivalent current function from the magnetic perturbation data. We use the method of *Richmond and Baumjohann* [1984] to separate the internal and external magnetic effects and to continue upward the external component to 110-km altitude. Figure 1 shows the resultant equivalent current function in Kiruna coordinates, which are defined by *Küppers et al.* [1979]. The origin is at Kiruna, and the  $y$  (eastward) axis is parallel to a contour of constant corrected geomagnetic latitude at Kiruna, with the  $x$  (northward) and  $z$  (downward) axes orthogonal to the  $y$  axis. The equivalent current function is represented by a two-dimensional Fourier series valid over the region  $x = -1100$  km in the south to  $x = 1100$  km in the north and  $y = -1300$  km in the west to  $y = 900$  km in the east. We choose these same boundaries for our calculations, although for display purposes a smaller region within these boundaries (the smaller rectangle in Figure 1) is used to avoid the distracting edge effects associated with the somewhat arbitrarily imposed boundary conditions. The equivalent current function is defined to be zero at the northern boundary and to have a vanishing normal derivative at the other three boundaries [see *Richmond and Baumjohann*, 1984]. We assume that the equivalent current system function is representative of a three-dimensional current system composed of a thin layer of hori-

zontal ionospheric currents centered at 110 km, coupled with magnetic-field-aligned currents above the ionosphere, flowing vertically along the  $z$  direction. We neglect the fact that the magnetic field direction deviates  $10^\circ$ – $15^\circ$  from the vertical.

The ionospheric current, with a height-integrated density  $\mathbf{K}$ , is assumed to obey Ohm's Law with a negligible dynamo effect from neutral winds:

$$\mathbf{K} = \Sigma_P \mathbf{E} + \Sigma_H \hat{z} \times \mathbf{E} \quad (1)$$

where  $\Sigma_P$  and  $\Sigma_H$  are the Pedersen and Hall conductances,  $\mathbf{E}$  is the horizontal electric field, and  $\hat{z}$  is a unit downward vector. The equivalent current differs from the true current and is expressed in terms of the equivalent current function  $\psi$  as

$$\mathbf{K}_{\text{equiv}} = -\hat{z} \times \nabla \psi \quad (2)$$

The electric field can reasonably be taken as electrostatic and related to a potential  $\Phi$  as

$$\mathbf{E} = -\nabla \Phi \quad (3)$$

Our assumption that field-aligned currents are strictly vertical allows us to equate the curls of  $\mathbf{K}$  and  $\mathbf{K}_{\text{equiv}}$  [e.g., *Matveev and Shpynev*, 1975], yielding

$$\Sigma_H \nabla^2 \Phi + \nabla \Sigma_H \cdot \nabla \Phi + \hat{z} \cdot \nabla \Sigma_P \times \nabla \Phi = \nabla^2 \psi \quad (4)$$

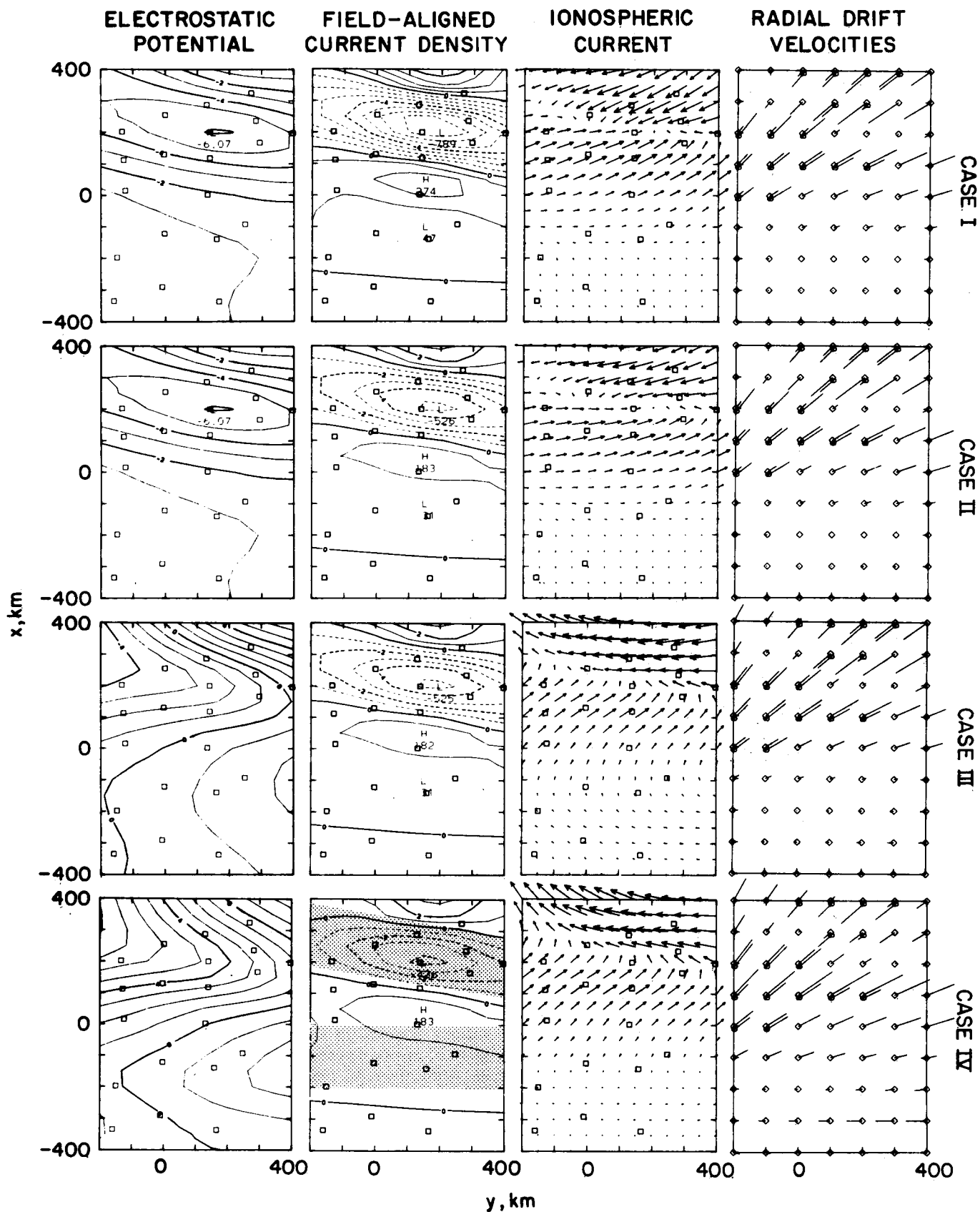


Fig. 2. Electrodynamics parameters for four trial computations, labeled cases I-IV. The area plotted in each frame corresponds to the inner rectangle in Figure 1. Squares in the first three columns show magnetometer locations; ovals in the fourth column show locations of radar line-of-sight drift measurements. First column: electrostatic potential in kilovolts (contour interval is 1 kV). Second column: downward field-aligned current in microamperes per square meter (contour interval is  $1 \mu\text{A}/\text{m}^2$ ; dashed contours show upward current). In case IV, shaded areas are regions of conductivity gradients (see text). Third column: height-integrated horizontal current density (a vector of length 100 km represents 1 A/m). Fourth column: observed and computed line-of-sight plasma drifts with respect to the radar (a vector of length 100 km represents 400 m/s). A diamond represents the head of the computed velocity component vector at that location; an oval represents the head of the measured velocity component vector at that location, following the directional convention of Baumjohann et al. [1978].

which is a second-order elliptic partial differential equation for  $\Phi$  in terms of the conductances and the equivalent current function. To solve (4) for the electrostatic potential  $\Phi$ , we need a conductivity model and a specification of boundary conditions, described in following sections. Numerically, we solve (4) by expressing derivatives as finite differences over a grid with 50-km spacings in the  $x$  and  $y$  directions and by using iterative overrelaxation, to compute the potential at each point in terms of values at neighboring points. About 500 iterations are required to achieve good convergence for the most complicated case (case IV).

When the potential has been determined, the electric field is computed from (3), and the ionospheric current is computed from (1). These in turn provide two related quantities of interest. First, the plasma drift velocity in the radar line of sight is

$$V_r = \hat{r} \cdot \mathbf{E} \times \mathbf{B}/B^2 = \hat{r} \cdot \mathbf{E} \times \hat{z}/B \quad (5)$$

where  $B$  is the geomagnetic field strength and  $\hat{r}$  is a unit horizontal vector directed outward from the radar located at  $x = -307$  km,  $y = -578$  km. Second, the downward field-aligned current density  $j_z$  is just the divergence of the ionospheric current:

$$j_z = \nabla \cdot \mathbf{K} \quad (6)$$

In the following sections we describe calculations for different conductivities and different boundary conditions on  $\Phi$ . The electrodynamic results are displayed in Figure 2, for the area within the small rectangle of Figure 1. The first column of Figure 2 shows the electrostatic potential  $\Phi$ . The second column shows the field-aligned current  $j_z$ . The third column shows the height-integrated horizontal ionospheric current  $\mathbf{K}$ . The fourth column shows a comparison between calculated and observed line-of-sight drifts with respect to the radar. The four rows of Figure 2 correspond to the four cases described below.

#### CASES I AND II: UNIFORM CONDUCTANCES, HOMOGENEOUS BOUNDARY CONDITIONS

If we assume that  $\Sigma_P$  and  $\Sigma_H$  have no gradients and that  $\Phi$  varies on boundaries as  $\psi/\Sigma_H$ , then the solution of (4) is trivial:

$$\Phi = \psi/\Sigma_H \quad (7)$$

$$j_z = -(\Sigma_P/\Sigma_H)\nabla^2\psi \quad (8)$$

For case I we use  $\Sigma_P = 15$  S and  $\Sigma_H = 20$  S, while for case II we use  $\Sigma_P = 10$  S and  $\Sigma_H = 20$  S. A Hall to Pedersen conductance ratio of the order of 2 is consistent with observations [e.g., Brekke *et al.*, 1974; Banks and Doupnik, 1975; Sulzbacher *et al.*, 1980; Vickrey *et al.*, 1981; Brüning *et al.*, 1981]. The Hall conductance was chosen to provide computed line-of-sight drifts with comparable magnitudes to the observed drifts, as seen in the fourth column of Figure 2 (first two rows). The electric potential (first column) is essentially identical for cases I and II, apart from computational inaccuracies. The currents differ, however. The larger Pedersen conductance in case I causes stronger divergent flow in the ionosphere, coupled with stronger field-aligned currents. As can be predicted from (8), the pattern of  $j_z$  is the same for the two cases, although the magnitude of  $j_z$  varies with  $\Sigma_P$ .

#### CASE III: UNIFORM CONDUCTANCES, WESTWARD ELECTRIC FIELD AT THE NORTHERN BOUNDARY

Electric field observations in the vicinity of the Harang discontinuity generally show a large-scale westward component

of the order of 10 mV/m or more [e.g., Wedde *et al.*, 1977; Horwitz *et al.*, 1978; Nielsen and Greenwald, 1979; Baumjohann *et al.*, 1980; Kamide and Vickrey, 1983]. The results for cases I and II do not show a westward field component of this magnitude. We can introduce a large-scale westward field component into the calculations by changing the boundary conditions on  $\Phi$ , most simply by retaining the same boundary conditions in the west, south, and east as for cases I and II (zero normal derivative of  $\Phi$ ) but imposing a potential gradient along the northern boundary as

$$\Phi(1100 \text{ km}, y) = A \cos [\pi(y + 1300 \text{ km})/2200 \text{ km}] \quad (9)$$

where  $A$  is an adjustable amplitude parameter. With uniform conductances an analytic solution to (4) can be obtained as

$$\Phi = \psi/\Sigma_H + A \{ \cos [\pi(y + 1300 \text{ km})/2200 \text{ km}] \cdot \cosh [\pi(x + 1100 \text{ km})/2200 \text{ km}] \} \cdot \{ \cosh \pi \}^{-1} \quad (10)$$

We choose a value of  $-25$  kV for  $A$  to yield an additional westward electric field component of about 9 mV/m in the Harang discontinuity region. Using the same conductances as case II ( $\Sigma_P = 10$  S,  $\Sigma_H = 20$  S), we obtain the distributions of potential, ionospheric currents, and field-aligned currents shown in the third row of Figure 2. The agreement between computed and observed line-of-sight drifts is still reasonable, though not greatly improved over cases I and II. Although the electric field and ionospheric current are different from case II, the field-aligned current is the same. In other words, the changed boundary conditions do not affect the divergence (nor the curl) of the ionospheric current within the boundaries when conductances are uniform.

#### CASE IV: NONUNIFORM CONDUCTANCES, WESTWARD ELECTRIC FIELD AT THE NORTHERN BOUNDARY

Our final case is designed to provide a qualitative picture of how conductance gradients can affect the results. Since we have no direct information about ionospheric conductivities during this period, we construct a simple conductance model based on features of the equivalent current pattern. Three regions of differing equivalent current characteristics are apparent within the small rectangle in Figure 1: weak currents in the south, an eastward electrojet in the upper middle, and a westward electrojet in the north. We assume a plausible conductance model with low conductances in the south, moderate conductances in the eastward electrojet, and higher conductances in the westward electrojet, the latter feature consistent with measurements showing generally larger conductivities in regions of westward auroral ionospheric current than in regions of eastward current [e.g., Wedde *et al.*, 1977; Horwitz *et al.*, 1978; Ahn *et al.*, 1983; Kamide and Vickrey, 1983]. Specifically, we use

$$\Sigma_H = 5 \text{ S} \quad x < -200 \text{ km}$$

$$\Sigma_H = 15 \text{ S} \quad 0 \text{ km} < x < 150 \text{ km} - y/6$$

$$\Sigma_H = 30 \text{ S} \quad 350 \text{ km} - y/6 < x$$

with exponential variations between these three regions of constant conductance. For simplicity of comparison with cases II and III, the Pedersen conductance is fixed everywhere at one-half the Hall conductance. The two regions where conductance gradients occur are shaded in the frame for  $j_z$  in Figure 2.

A comparison between cases III and IV in Figure 2 shows that  $\Phi$  and  $\mathbf{K}$  differ to some extent over the entire plotting region, whereas  $j_z$  differs only in those regions where conduc-

tance gradients exist in case IV. To see why this happens, let us further manipulate (1). By solving (1) for  $\mathbf{E}$  in terms of  $\mathbf{K}$  and rearranging, we get

$$\mathbf{K} = \frac{\Sigma_H}{\Sigma_P} \hat{z} \times \mathbf{K} + \Sigma_C \mathbf{E} \quad (11)$$

$$\Sigma_C = \Sigma_P + \Sigma_H^2 / \Sigma_P \quad (12)$$

where  $\Sigma_C$  is the Cowling conductance. Taking the curl of (11) and equating it to the curl of (2) yield

$$-\frac{\Sigma_H}{\Sigma_P} j_z - \mathbf{K} \cdot \nabla \left( \frac{\Sigma_H}{\Sigma_P} \right) + \hat{z} \cdot \mathbf{E} \times \nabla \Sigma_C = \nabla^2 \psi \quad (13)$$

In all regions where conductance gradients vanish, (13) gives the same field-aligned current as (8), which was derived for the case of conductances uniform everywhere. Inspection of (13) also explains the modest reduction in intensity of upward field-aligned current for case IV with respect to case III in the shaded region between the eastward and westward electrojets: the westward component of  $\mathbf{E}$  combined with the northward gradient of  $\Sigma_C$  means that  $\hat{z} \cdot \mathbf{E} \times \nabla \Sigma_C$  is positive, so that this term tends to offset partially  $\nabla^2 \psi$  in this region. Case IV line-of-sight drifts compare less favorably with observations than do those for case III.

#### DISCUSSION

The sensitivity of computed ionospheric electrostatics to the conductivity model in this regional analysis appears to be comparable to sensitivity that has been seen in global analyses [e.g., Kamide and Richmond, 1982]. However, an additional complication arises in the regional analysis that has no counterpart in global analyses. Either a global analysis has no boundary (if the entire globe is analyzed), or else the boundary of the analysis can be placed in a region where electric fields are sufficiently small (e.g., the equator) that their accurate specification on this boundary is unimportant. By contrast, the specification of boundary conditions in a regional analysis can have an important influence on the results, as we have demonstrated. This requires that some independent information about the electric fields be available, either in the form of measurements or in the form of general knowledge of electric field behavior (e.g., the fact that there tends to be a westward component around the Harang discontinuity).

Although our primary purpose here is not to try to determine the actual ionospheric electrodynamic conditions for the example analyzed, the results of these calculations, along with those of other cases not displayed here, do appear to point to the necessity of a significant upward field-aligned current near the boundary between the eastward and westward electrojets. Even though some cases we tried involving conductivity gradients in this region resulted in reduced upward current (e.g., case IV versus case III), we were not able to eliminate this current under any reasonable combination of boundary conditions and conductivity models without totally destroying the agreement between observed and calculated line-of-sight drifts. Whether or not significant field-aligned currents in the Harang discontinuity region are a regular feature has not been established in the existing scientific literature. Baumjohann et al. [1980], Kamide [1982], and Kamide and Vickrey [1983] have suggested that significant field-aligned currents may be present in the Harang discontinuity only during certain conditions.

*Acknowledgments.* The Scandinavian Magnetometer Array observations and the work of W.B. were financially supported by grants

from the Deutsche Forschungsgemeinschaft. The National Center for Atmospheric Research is sponsored by the National Science Foundation.

The Editor thanks Y. Kamide and J. C. Foster for their assistance in evaluating this paper.

#### REFERENCES

- Ahn, B.-H., R. M. Robinson, Y. Kamide, and S.-I. Akasofu, Electric conductivities, electric fields and auroral particle energy injection rate in the auroral ionosphere and their empirical relations to the horizontal magnetic disturbances, *Planet. Space Sci.*, **31**, 641–653, 1983.
- Banks, P. M., and J. R. Doupnik, A review of auroral zone electrostatics deduced from incoherent scatter radar observations, *J. Atmos. Terr. Phys.*, **37**, 951–972, 1975.
- Baumjohann, W., R. A. Greenwald, and F. Küppers, Joint magnetometer array and radar backscatter observations of auroral currents in northern Scandinavia, *J. Geophys.*, **44**, 373–383, 1978.
- Baumjohann, W., J. Untiedt, and R. A. Greenwald, Joint two-dimensional observations of ground magnetic and ionospheric electric fields associated with auroral zone currents, 1, Three-dimensional current flows associated with a substorm-intensified eastward electrojet, *J. Geophys. Res.*, **85**, 1963–1978, 1980.
- Bazarchapov, A. D., V. M. Mishin, D. Sh. Shirapov, and G. B. Shpynev, Electric fields and currents in the quiet magnetosphere as determined from ground measurements, *Issled. Geomagn. Aeron. Fiz. Solntsa*, **46**, 13–28, 1979.
- Belov, B. A., R. G. Afonina, A. E. Levitin, D. C. Fayermark, and Ya. I. Fel'dsteyn, Three-dimensional current systems of geomagnetic field variations in the northern polar cap associated with the components of the interplanetary magnetic field vector, *Geomagn. Aeron. Engl. Transl.*, **18**, 475–477, 1978.
- Brekke, A., J. R. Doupnik, and P. M. Banks, Incoherent scatter measurements of E region conductivities and currents in the auroral zone, *J. Geophys. Res.*, **79**, 3773–3790, 1974.
- Brüning, K., W. Baumjohann, K. Wilhelm, W. Stüdemann, A. Urban, W. Ott, K. Spencer, G. L. Schmidtke, and H. M. Fischer, Application of different methods for the determination of ionospheric conductivities from sounding rocket observations, *J. Geophys.*, **49**, 74–81, 1981.
- Fayermark, D. S., Reconstruction of the three-dimensional current system of the high-latitude region from ground-based geomagnetic measurements, *Geomagn. Aeron. Engl. Transl.*, **17**, 114–115, 1977.
- Feldstein, Y. I., R. G. Afonina, B. A. Belov, and A. E. Levitin, Magnetic field and field-aligned current variations in the polar cusp controlled by interplanetary medium parameters, *Planet. Space Sci.*, **30**, 635–640, 1982.
- Feldstein, Y. I., A. E. Levitin, D. S. Faermark, R. G. Afonina, B. A. Belov, and V. Y. Gaidukov, Electric fields and potential patterns in the high-latitude ionosphere for different situations in interplanetary space, *Planet. Space Sci.*, **32**, 907–923, 1984.
- Friis-Christensen, E., Y. Kamide, A. D. Richmond, and S. Matsushita, Interplanetary magnetic field control of high-latitude electric fields and currents determined from Greenland magnetometer data, *J. Geophys. Res.*, **90**, 1325–1328, 1985.
- Harang, L., The mean field of disturbance of polar geomagnetic storms, *Terr. Magn. Atmos. Electr.*, **51**, 353–380, 1946.
- Heppner, J. P., The Harang discontinuity in auroral belt ionospheric currents, *Geophys. Publ.*, **29**, 105–120, 1972.
- Horwitz, J. L., J. R. Doupnik, and P. M. Banks, Chatanika radar observations of the latitudinal distribution of auroral zone electric fields, conductivities, and currents, *J. Geophys. Res.*, **83**, 1463–1481, 1978.
- Kamide, Y., The relationship between field-aligned currents and the auroral electrojets: A review, *Space Sci. Rev.*, **31**, 127–243, 1982.
- Kamide, Y., and A. D. Richmond, Ionospheric conductivity dependence of electric fields and currents estimated from ground magnetic observations, *J. Geophys. Res.*, **87**, 8331–8337, 1982.
- Kamide, Y., and A. D. Richmond, Estimation of electric fields and currents from ground-based magnetometer data, in *Magnetospheric Currents*, *Geophys. Monogr. Ser.*, vol. 28, edited by T. A. Potemra, pp. 67–76, AGU, Washington, D. C., 1983.
- Kamide, Y., and J. F. Vickrey, Variability of the Harang discontinuity as observed by the Chatanika radar and the IMS Alaska magnetometer chain, *Geophys. Res. Lett.*, **10**, 159–162, 1983.
- Kamide, Y., A. D. Richmond, and S. Matsushita, Estimation of ionospheric electric fields, ionospheric currents, and field-aligned currents from ground magnetic records, *J. Geophys. Res.*, **86**, 801–813, 1981.

- Kamide, Y., B.-H. Ahn, S.-I. Akasofu, W. Baumjohann, E. Friis-Christensen, H. W. Kroehl, H. Maurer, A. D. Richmond, G. Rostoker, R. W. Spiro, J. K. Walker, and A. N. Zaitzev, Global distribution of ionospheric and field-aligned currents during substorms as determined from six IMS meridian chains of magnetometers: Initial results, *J. Geophys. Res.*, **87**, 8228–8240, 1982.
- Kern, J. W., Analysis of polar magnetic storms, *J. Geomagn. Geoelectr.*, **18**, 125–131, 1966.
- Küppers, F., J. Untiedt, W. Baumjohann, K. Lange, and A. G. Jones, A two-dimensional magnetometer array for ground-based observations of auroral zone electric currents during the International Magnetospheric Study (IMS), *J. Geophys.*, **46**, 429–450, 1979.
- Levitin, A. E., B. A. Belov, R. G. Afonina, D. S. Fayermark, and Y. I. Feldstein, Three-dimensional current systems in the north polar cap for different types of geomagnetic field variations, in *Variations of Geomagnetic Field and the Aurora* (in Russian), edited by Y. I. Feldstein, pp. 86–106, Izmiran, Moscow, 1977.
- Levitin, A. E., R. G. Afonina, B. A. Belov, and Ya. I. Feldstein, Geomagnetic variation and field-aligned currents at northern high-latitudes, and their relations to the solar wind parameters, *Philos. Trans. R. Soc. London Ser. A*, **304**, 253–301, 1982.
- Matveev, M. I., and G. V. Shpynev, Determination of electric fields and field-aligned currents in the magnetosphere on data of geomagnetic variations, *Issled. Geomagn. Aeron. Fiz. Solntsa*, **36**, 34–39, 1975.
- Mishin, V. M., and G. V. Popov, On field-aligned currents in magnetosphere, *Issled. Geomagn. Aeron. Fiz. Solntsa*, **8**, 3–28, 1969.
- Mishin, V. M., M. I. Matveev, G. B. Shpynev, A. D. Bazarzhapov, and V. Kh. Kompanetz, Preliminary results of calculations of three-dimensional electric current system in the magnetosphere using ground-based data of geomagnetic disturbances, *Issled. Geomagn. Aeron. Fiz. Solntsa*, **43**, 14–17, 1977.
- Mishin, V. M., A. D. Bazarzhapov, and G. B. Shpynev, Electric fields and currents in the earth's magnetosphere, in *Dynamics of the Magnetosphere*, edited by S.-I. Akasofu, pp. 249–268, D. Reidel, Hingham, Mass., 1979.
- Mishin, V. M., G. B. Shpynev, and A. D. Bazarzhapov, Large-scale electric field and currents in the high-latitude ionosphere and magnetosphere as a function of solar wind parameters, *Adv. Space Res.*, **1**, 159–169, 1981.
- Nielsen, E., and R. A. Greenwald, Electron flow and visual aurora at the Harang discontinuity, *J. Geophys. Res.*, **84**, 4189–4200, 1979.
- Nielsen, E., and K. Schlegel, A first comparison of STARE and EISCAT electron drift velocity measurements, *J. Geophys. Res.*, **88**, 5745–5750, 1983.
- Richmond, A. D., and W. Baumjohann, Three-dimensional analysis of magnetometer array data, *J. Geophys.*, **54**, 138–156, 1984.
- Sulzbacher, H., W. Baumjohann, and T. A. Potemra, Coordinated magnetic observations of morning sector auroral zone currents with Triad and the Scandinavian Magnetometer Array: A case study, *J. Geophys.*, **48**, 7–17, 1980.
- Vickrey, J. F., R. R. Vondrak, and S. J. Matthews, The diurnal and latitudinal variation of auroral zone ionospheric conductivity, *J. Geophys. Res.*, **86**, 65–75, 1981.
- Wedde, T., J. R. Doupnik, and P. M. Banks, Chatanika observations of the latitudinal structure of electric fields and particle precipitation on November 21, 1975, *J. Geophys. Res.*, **82**, 2743–2751, 1977.

---

W. Baumjohann, Max-Planck-Institut für Physik und Astrophysik, Institut für extraterrestrische Physik, D-8046 Garching, Federal Republic of Germany.

S. Matsushita and A. D. Richmond, National Center for Atmospheric Research, P.O. Box 3000, Boulder, CO 80307.

M. Murison, Department of Astronomy, University of Wisconsin, Madison, WI 53706.

(Received September 7, 1984;  
revised December 12, 1984;  
accepted December 13, 1984.)